A PM3-SRP + Analytic Function Potential Energy Surface Model for O(³P) Reactions with Alkanes. Application to O(³P) + Ethane†

Tianying Yan,‡,§ Charles Doubleday,*,‖ and William L. Hase*,⊥

Department of Chemistry, Wayne State University, Detroit, Michigan 48202,
Department of Chemistry, Columbia University, New York, New York 10027, and
Department of Chemistry and Biochemistry, Texas Tech University, Lubbock, Texas 79409-1061

The PM3 semiempirical electronic structure theory is reparametrized with specific reaction parameters (SRPs) to develop a potential energy surface (PES) for O(³P) processing of alkanes. The results of high-level ab initio calculations for the O(³P) + C₂H₆ primary reactions, yielding OH + C₂H₅, C₂H₅O + H, and CH₃O + CH₃, 11 ensuing secondary and unimolecular dissociation reactions involving products of these primary reactions, and additional reactions were used to develop two PM3-SRP models for the PES. The ab initio results used for this fitting were taken from previous multiconfiguration calculations and additional PMP2/cc-pVTZ calculations reported here. Even though these two PM3-SRP models are unable to quantitatively represent the many reactions that occur in high-energy collisions of O(³P) with alkanes, they are vast improvements over the PES of PM3 theory. These models are used in direct dynamics classical trajectory simulations of the O(³P) + C₂H₆ reaction at a 5 eV collision energy. The results of the simulations show that the products of the three primary reactions are highly excited and are able to undergo a large number of ensuing secondary and unimolecular dissociation reactions, and long-time trajectory integrations are required to study these many product channels. The large internal excitations of the primary reactions' products agree with results of a previous MSINDO direct dynamics trajectory study. Reaction cross sections calculated for the primary reaction channels are also in good agreement with the MSINDO results. Velocity scattering angles, calculated for products of the secondary and unimolecular dissociation channels, provide detailed information concerning the molecular dynamics of these products. They are formed directly and also via long-lived intermediates.

I. Introduction

Low-energy collisions of electronic-ground-state oxygen atoms O(³P) with hydrocarbons are important in combustion and atmospheric chemistry.[1–3] At low energies, the only reaction for O(³P) plus an alkane is abstraction giving OH· + R·.[1] Low-energy collisions of O(³P) with hydrocarbon surfaces are important in a variety of contexts ranging from the fabrication of polymers for the microelectronics industry[4] to the processing of hydrocarbon films on the surface of atmospheric aerosols.[5] Recent experiments[6,7] and simulations[8] have probed the dynamics of the low-energy reaction of O(³P) atoms with hydrocarbon interfaces.

Interest in high-energy collisions of O(³P) with hydrocarbons has been motivated by the erosion of polymeric coatings on the surface of spacecraft in low Earth orbit (LEO).[9] Spacecraft in LEO travel at a velocity of approximately 8 km/s, giving rise to a relative translational energy of ∼5 eV for O(³P) striking the spacecraft. Under such harsh conditions, there is considerable erosion of the spacecraft's surface. Minton and co-workers[6,10–12] pioneered the development of a molecular beam technique for studying the reaction of O(³P) atoms with hydrocarbons at high collision energies. At these energies, other reaction channels,

in addition to the above abstraction, are open for O(³P) atoms reacting with alkanes. From ab initio calculations, Massa and co-workers[13] found a C−C bond rupture pathway, which yields CH₃ + OCH₃ for O(³P) + C₂H₆. Schatz and co-workers[14,15] extended these calculations, using higher-level theory and performing a more exhaustive search of reaction pathways, and discovered a C−H bond rupture channel, i.e., O(³P) + RH → H + OR. For the O(³P) + C₂H₆ system, the threshold energy is about 2 eV for both the C−C and C−H bond rupture channels.[15] Most recently, we have used high-level multiconfiguration ab initio methods to investigate energetics, transition states, and intrinsic reaction coordinates for the O(³P) + hydrocarbon abstraction and bond rupture channels and secondary and unimolecular reactions of the radical products formed by these channels.[16]

Minton and co-workers studied hyperthermal reactions of O(³P) with CH₄, C₂H₆, and C₃H₈.[17] They observed the abstraction channel as well as the H−C and C−C rupture channels, yielding OH + R, H + OR, and R′O + R″, respectively. Schatz and co-workers[14,15] have simulated these experiments with direct dynamics simulations employing the MSINDO semiempirical Hamiltonian and B3LYP/6-31G* density functional theory. QM/MM direct dynamics simulations have been used to simulate O(³P) reaction with alkylthiolate self-assembled monolayers (SAMs) at both low[8] and high[18,19] collision energies.

At this time, a QM/MM model based on accurate ab initio theory is not a practical approach for modeling collisions and reactions of O(³P) with hydrocarbon surfaces. A large number of atoms must be included in the QM part of the model to

* To whom correspondence should be addressed. E-mail: ced3@columbia.edu (C.D.), bill.hase@ttu.edu (W.L.H.).
‡ Wayne State University.
§ Current address: Department of Chemistry and Henry Eyring Center for Theoretical Chemistry, University of Utah, Salt Lake City, UT 84112.
‖ Columbia University.
⊥ Texas Tech University.

TABLE 1: Comparison of MRCI, PM3, and PM3-SRP Reaction Energies[a,b]

| | MRCI | | PM3 | | PM3-SRP | | | |
| | | | | | model 1 | | model 2 | |
reaction[c]	$\Delta E^{\ddagger}_{ZPE}$	ΔE^{0}_{ZPE}	$\Delta E^{\ddagger}_{ZPE}$	ΔE^{0}_{ZPE}	$\Delta E^{\ddagger}_{ZPE}$	ΔE^{0}_{ZPE}	$\Delta E^{\ddagger}_{ZPE}$	ΔE^{0}_{ZPE}
$O(^3P) + CH_4 \rightarrow OH + CH_3$	10.5	1.4	7.0	−19.9	10.5	3.9	8.8	−8.7
$O(^3P) + C_2H_6 \rightarrow OH + C_2H_5$	9.0	−1.4	4.2	−27.8	7.0	−7.9	10.7	−16.0
$OH + C_2H_6 \rightarrow C_2H_5 + H_2O$	2.8	−18.0	5.4	−25.3	3.9	−14.3	7.6	−18.6
$OH + C_2H_5 \rightarrow H_2O + {^3}C_2H_4$	4.3	−17.8	7.0	−22.5	5.8	−12.8	8.9	−17.3
$OH + C_2H_5 \rightarrow H_2O + {^3}CH_3CH$	4.9	−10.2	5.1	−17.7	2.6	−9.5	7.9	−10.4
$O(^3P) + CH_3-CH_3 \rightarrow CH_3O + CH_3$	46.9	1.1	25.9	−29.1	47.2	3.0	51.3	−5.7
$O(^3P) + CH_3-CH_3 \rightarrow C_2H_5O + H^{d}$	48.3	11.8	24.4	−5.9	32.1	19.1	34.5	9.2

[a] Energies are in kcal/mol and include harmonic zero-point energies for the reactants, transition states, and products. The vibrational frequencies for the MRCI energies were calculated at the CASSCF/cc-pVTZ level of theo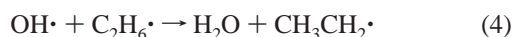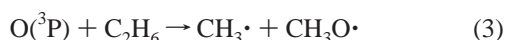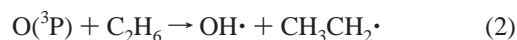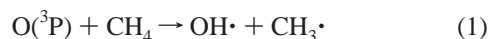ry with active space (10,10), (8,8), (9,9), (10,10), (8,8), and (4,4), respectively, for the first six reactions. [b] Experimental 0 K heats of reaction for reaction 1−3 and 6 are 2.1 ± 0.2, −5.5 ± 1.4, −21.8 ± 1.4, and −1.9 ± 1.0, respectively, for the first six reactions. [c] Reactions are on the ground-state triplet potential energy surface. [d] This reaction was not studied at the MRCI level of theory. The energies listed below MRCI are the PMP2 values discussed in the text. This reaction was not included in the PM3-SRP fitting for model 1.

accurately represent the many reaction sites and their multiple reaction channels. Only very low-level ab initio methods are computationally tractable for such a large system. As illustrated by the above two QM/MM studies, the use of a semiempirical QM component for the model is feasible. However, it is important to parametrize the semiempirical model so that it gives a potential energy surface that accurately represents the chemical reactions that might occur.

In the work presented here, the PM3-SRP model developed by Li et al.,[8] for $O(^3P)$ reacting with hydrocarbons, is refined and made more accurate by fitting potential energy surface properties determined from high-level multiconfiguration ab initio calculations reported previously,[16] as well as additional ab initio calculations presented here, for a set of reactions associated with $O(^3P)$ collisions with ethane. The reparametrization is supplemented by analytic functions to obtain an overall accurate fit to the high-level ab initio calculations. Two different fitting schemes are employed to determine the sensitivity of the derived potential to the fitting. The two resulting PM3-SRP models are then employed in QM direct dynamics simulations of $O(^3P)$ reaction with ethane at 5 eV. The trajectories are numerically integrated for a sufficiently long period of time to study secondary and unimolecular reactions that might occur.

II. PM3-SRP Model

A. Ab Initio Information. In previous work,[16] energetics, structures, and vibrational frequencies for the following six reactions were calculated at various levels of multiconfiguration electronic structure theory

$$O(^3P) + CH_4 \rightarrow OH\cdot + CH_3\cdot \quad (1)$$

$$O(^3P) + C_2H_6 \rightarrow OH\cdot + CH_3CH_2\cdot \quad (2)$$

$$O(^3P) + C_2H_6 \rightarrow CH_3\cdot + CH_3O\cdot \quad (3)$$

$$OH\cdot + C_2H_6\cdot \rightarrow H_2O + CH_3CH_2\cdot \quad (4)$$

$$OH\cdot + C_2H_5\cdot \rightarrow H_2\dot{C}-\dot{C}H_2 + H_2O \quad (5)$$

$$OH\cdot + C_2H_5\cdot \rightarrow CH_3\ddot{C}H + H_2O \quad (6)$$
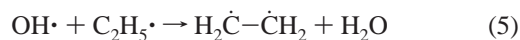
The first three are representative of primary reactions between $O(^3P)$ and gaseous and condensed-phase hydrocarbons. The remaining three are possible secondary abstraction reactions of the OH· product with a hydrocarbon surface to form H_2O.

The highest level of theory used to optimize geometries of the stationary points for the first two reactions and the remaining

four reactions is CASPT2/vtz and CASSCF/vtz, respectively.[16] Barrier heights and heats of reaction were calculated at these geometries using MRCI theory with the inclusion of the Davidson correction[20] for the quadrupole excitations and extrapolated to the complete basis set limit, i.e., MRCI+Q/CBL.[16] These MRCI energies for the six reactions are listed in Table 1.

The abstraction reaction forming OH is the only primary reaction channel at low collision energies, and only secondary reactions involving OH are of possible important for this energy regime. However, as described above, at higher energies, C−H and C−C bond ruptures become important primary reactions, and secondary and unimolecular reactions involving their radical products can occur. Listed in Figure 1 are barrier heights and heats of reaction for the three primary reaction channels and for secondary reactions involving the products of these channels. The energies not in parentheses are PMP2/cc-pVTZ//UMP2/cc-pVTZ values and were calculated as part of the work presented here. The energies in parentheses for channels P1, P3, S1, and S2 in Figure 1 are the MRCI values in Table 1. A comparison of the MRCI and PMP2 energies shows that PMP2 gives accurate barrier heights and heats of reaction as compared to those for the much higher MRCI theory. Thus, if energies required for the PM3-SRP fitting, described in the next section, were not determined by the MRCI calculation, then the PMP2 values were used.

For high-energy collisions between $O(^3P)$ and hydrocarbons, the products of the primary reactions can contain sufficient energy to undergo unimolecular dissociation reactions. Summarized in Figure 2 are possible unimolecular dissociation reactions for the radicals formed by the $O(^3P) + C_2H_6$ primary and secondary reactions shown in Figure 1.

Even though the reactions included in Figures 1 and 2 is an extensive list, it is possible that other reactions might occur in high-energy $O(^3P)$ + hydrocarbon collisions. Also, an exhaustive search was not made to identify all of the transition state (TS) structures for these reactions. For example, several higher TSs were reported by Schatz and co-workers[14] for the H−C and C−C bond-breaking channels P2 and P3.

B. Fitting PM3 to the ab Initio Information. Two semi-empirical potential energy surfaces (PESs) for $O(^3P) + C_2H_6$ were developed by refitting PM3[21,22] with specific reaction parameters (SRPs).[23,24] The UHF wave function of PM3, which has analytical derivatives, was used for this fitting. The PM3 Hamiltonian for the $O(^3P) + C_2H_6$ reactions has 47 parameters (i.e., 18, 18, and 11 for C, O, and H, respectively), and as described below, each of the parameters was modified

PES Model for O(^{3}P) Reactions with Alkanes

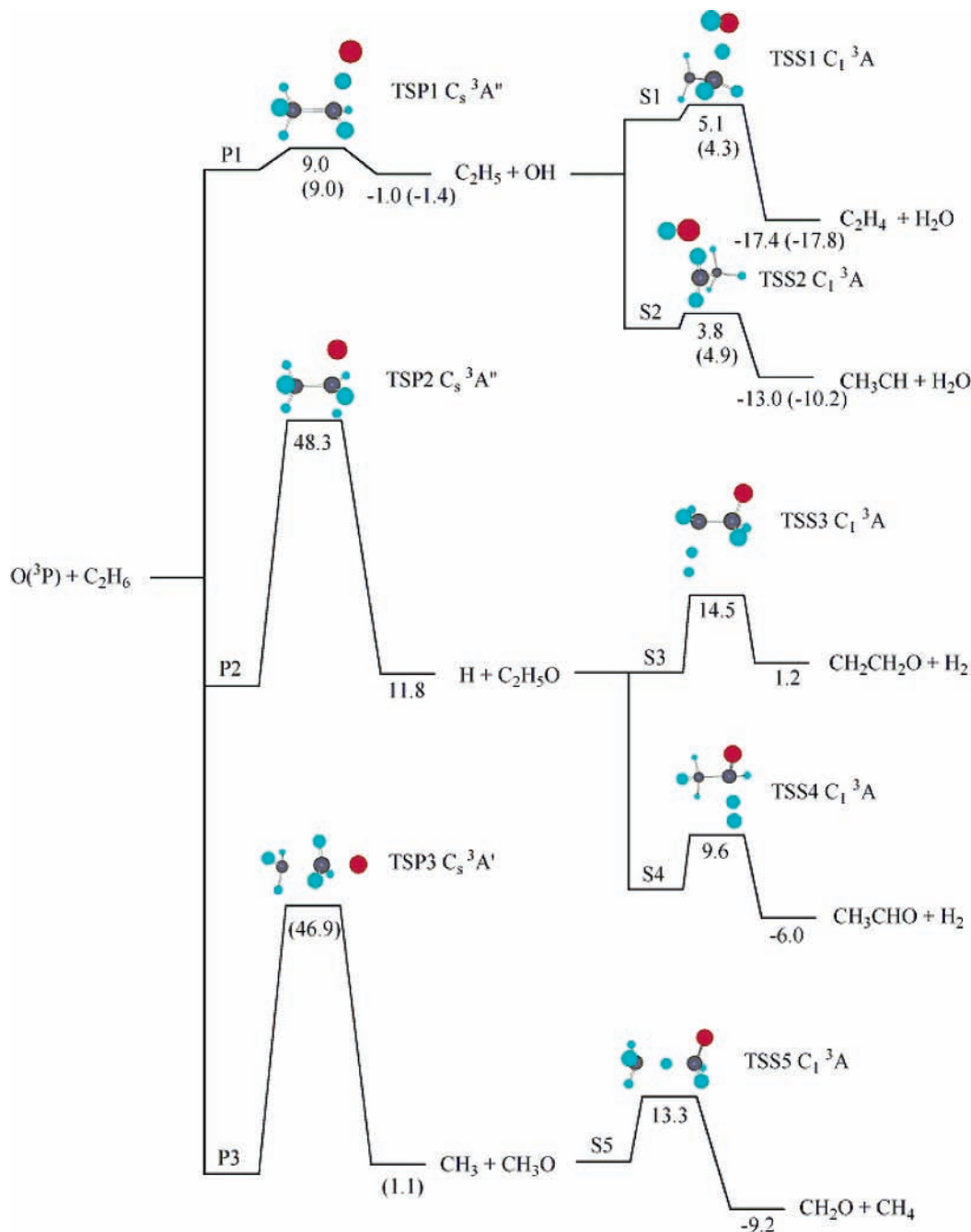*J. Phys. Chem. A, Vol. 108, No. 45, 2004* **9865**

Figure 1. Barrier heights and 0 K heats of reaction (including reactant, transition state, and product zero-point energies) for the three primary reactions and secondary reactions involving products of the primary reactions. Energies not in parentheses were calculated at the PMP2/cc-pVTZ// UMP2/cc-pVTZ level of theory. The energies in parentheses are the MRCI values from Table 1.

in the fitting. These parameters are accessible through the "EXTERNAL" keyword in MOPAC7.0.[25] An additional 32 parameters are introduced into the PM3-SRP model, giving a total of 79 parameters, by expressing the resonance integrals as

$$H_{ij}^{uv} = \chi_{ij}^{uv}(r_{ij})H_{ij}^{0,uv} \tag{7}$$

where $\chi_{ij}^{uv}(r_{ij})$ is a distance-dependent scaling term,[26,27] r_{ij} is the distance between atoms i and j, and

$$H_{ij}^{0,uv} = \frac{1}{2}(\beta_u + \beta_v)S_{uv} \tag{8}$$

is the PM3 resonance integral between atoms i and j. Here, uv labels the overlap type (ss, sp, pp), and S_{uv} is the overlap integral

between atoms i and j.[28] The distance-dependent scaling term

$$\chi_{ij}^{ab}(r_{ij}) = \chi_{ij,\text{small}}^{ab} + \frac{1}{2}(\chi_{ij,\text{large}}^{ab} - \chi_{ij,\text{small}}^{ab})\{1 + \tanh[f_{ij}(r_{ij} - r_{ij}^0)]\} \tag{9}$$

switches from $\chi_{ij,\text{small}}^{ab}$ at small values of r_{ij} to $\chi_{ij,\text{large}}^{ab}$ at large r_{ij}. r_{ij}^0 is the distance at which the switching function is turned on halfway, and f_{ij} governs the rate at which the switch is turned on. There are 11 modified resonance integrals, i.e., s,s for H,H; s,s and s,p for O,H and C,H; and s,s, s,p, and p,p for C,O and C,C. The scaling terms of the modified resonance integrals for a particular atom pair (e.g., the three C,C resonance integrals) all have the same f_{ij} and r_{ij}^0 parameters. With this constraint, there are 32 parameters associated with the resonance terms in
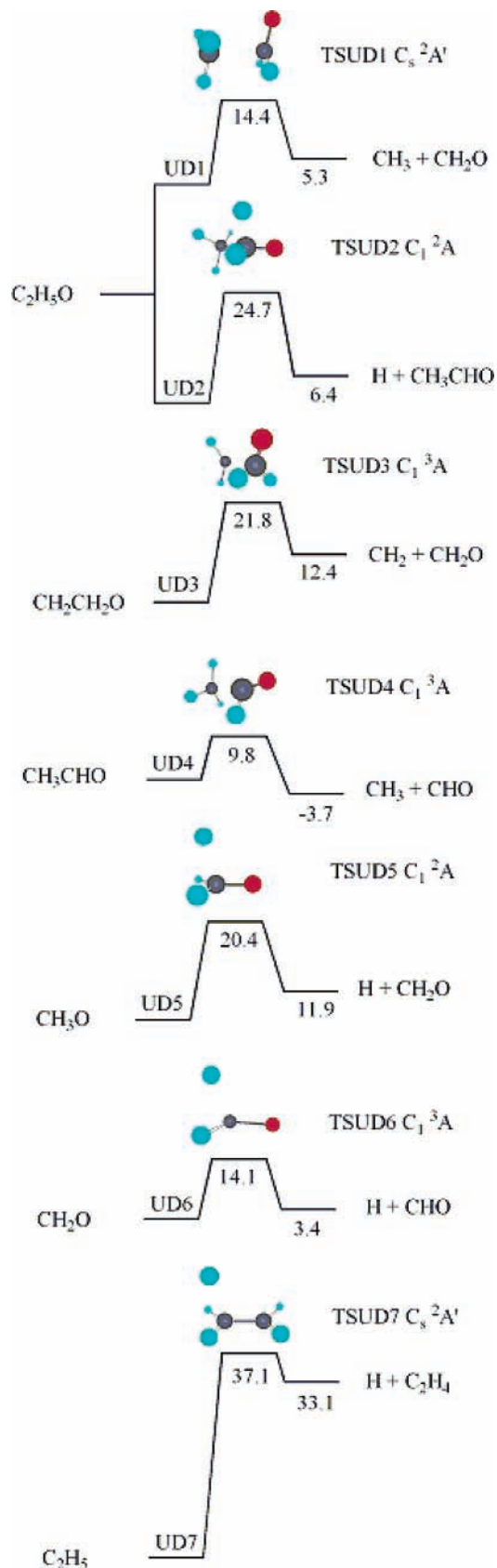
Figure 2. Barrier heights and 0 K heats of reaction (including reactant, transition state, and product zero point energies) for unimolecular dissociations of some of the products of the primary and secondary reactions in Figure 1. The energies were calculated at the PMP2/cc-pVTZ//UMP2/cc-pVTZ level of theory.

eq 9. The off-diagonal, one-electron integrals in the Fock matrix are responsible for bond formation/dissociation in chemical

reactions. Therefore, with these additional parameters for the resonance integrals in the SRP fitting, potential energy surface properties for the $O(^3P) + C_2H_6$ system are better represented.

A Fortran genetic algorithm program[29] is interfaced with MOPAC7.0,[25] with distance-dependent scaling factors,[29] to minimize the following weighted sum of squares

$$w_E \sum_i (E_i^{PM3} - E_i^0)^2 + w_L \sum_i (L_i^{PM3} - L_i^0)^2 +$$
$$w_A \sum_i (A_i^{PM3} - A_i^0)^2 + w_D \sum_i (D_i^{PM3} - D_i^0)^2 \quad (10)$$

where the difference terms involve PM3-SRP values minus ab initio values for energies, bond lengths, bond angles, and dihedral angles. The w terms are weighting factors to emphasize the importance of fitting particular energies and geometries.

Here, we adopt the philosophy of the PM3 parametrization[21] and simultaneously fit energies and geometries, for a series of reactions, using the 79 PM3-SRP parameters described above. The original PM3 parameters listed in Table 2 are very good initial guesses for our SRP reparametrization and are allowed to be changed within 5% of their original values in the fitting. The terms $\chi_{ij,large}^{ab}$ and $\chi_{ij,small}^{ab}$ used in the distance-dependent scaling factors are constrained between 0.5 and 1.5. The r_{ij}^0s are constrained within $0.9-2.0$ times the equivalent bond lengths between atoms i and j. The molecules from which the ranges for the r_{ij}^0 values are determined are C_2H_6 for $C-C$ and $C-H$, OH radical for $O-H$, H_2 for $H-H$, and CH_2O for $C-O$. The f_{ij} factors, which govern the steepness of the switching function, are constrained between 1.0 and 5.0.

Two PM3-SRP models, i.e., models 1 and 2, for the $O(^3P) + C_2H_6$ PES were developed by fitting structures and energies of reactant, transition state, and product stationary points for two groups of the reactions described above. For model 1, the MRCI energies and structures of the stationary points for only six reactions, i.e., reactions $1-6$, were fit. Model 2 has a much more extensive fitting, with the PMP2 energies and structures for 14 reactions included in the fit, i.e., all of the reactions in Figures 1 and 2 were fit except reaction UD7 in Figure 2. The fitting for model 2 also included the short-range repulsive potential between $O(^3P) + CH_4$ (described below), to ensure that this component of the nonbonding and nonreactive potential between $O(^3P)$ and alkanes is correctly represented. Model 2 was developed after trajectory simulations of $O(^3P) + C_2H_6$ collisions (discussed below) showed the participation of many different reactions. Tables 2 and 3 give the PM3-SRP parameters and the distance-dependent scaling factors, respectively, for models 1 and 2.

A comparison between the PM3-SRP model 1 and the MRCI ab initio results is given by the first six reactions in Table 1. Stationary-point structures and energies were used for only these six reactions to derive the SRP parameters for model 1. Overall, there is good agreement between the model 1 and MRCI energetics. The two largest discrepancies are in the heats of reaction for reactions 1 and 2. The differences in the model 1 and MRCI barriers are 5 kcal/mol or less. PM3-SRP model 1 is a vast improvement over the PM3 energetics for these six reactions. However, it is troublesome that, for model 1, in which energies for only six reactions are fit, the heat of reaction for reaction 1 is not well fit. This is not an important issue for the high-energy simulations reported here, but it does mean that model 1 is not adequate for simulating product energy partitioning in low-energy $O(^3P) + C_2H_6$ collisions.

PES Model for O(^{3}P) Reactions with Alkanes

J. Phys. Chem. A, Vol. 108, No. 45, 2004 **9867**

TABLE 2: List of PM3 and PM3-SRP Parameters

PM3 parameter	H atom			C atom			O atom		
		PM3-SRP			PM3-SRP			PM3-SRP	
	PM3	model 1	model 2	PM3	model 1	model 2	PM3	model 1	model 2
U_{ss}	−13.073321	−12.713245	−13.128892	−47.270320	−47.7281129	−48.377744	−86.993002	−89.3648403	−88.267433
U_{pp}				−36.266918	−38.3942174	−35.687775	−71.879580	−74.1011413	−71.683103
β_s	−5.626512	−5.7139669	−5.570756	−11.910015	−11.8605071	−11.993243	−45.202651	−43.7808448	−45.804161
β_p				−9.802755	−9.4413274	−9.638305	−24.752515	−25.9694874	−25.163959
ζ_s	0.967807	0.9747437	0.990713	1.565085	1.5359511	1.557473	3.796544	3.8238235	3.847996
ζ_p				1.842345	1.7961893	1.799748	2.389402	2.3294996	2.393266
α	3.356386	3.1445129	3.403693	2.707807	2.8023882	2.705665	3.217102	3.1158375	3.261432
G_{ss}	14.794208	13.8182036	14.596692	11.200708	10.9780099	11.449629	15.755760	15.5534583	15.802380
G_{sp}				10.265027	10.7273987	10.324418	10.621160	10.9893146	10.699932
G_{pp}				10.796292	10.9024625	10.902681	13.654016	14.7457604	13.883658
G_{p2}				9.042566	9.1988949	8.908248	12.406095	12.6024701	12.247488
H_{sp}				2.290980	2.1635088	2.319499	0.593883	0.5905295	0.595978
a_1	1.128750	1.0667778	1.149482	0.050107	0.0513551	0.049790	−1.131128	−1.0745888	−1.127537
b_1	5.096282	4.8911326	5.170553	6.003165	6.4024037	5.930750	6.002477	5.8165331	6.084215
c_1	1.537465	1.5434240	1.529827	1.642214	1.5729843	1.663760	1.607311	1.5446585	1.605593
a_2	−1.060329	−1.0303214	−1.064338	0.050733	0.0540469	0.051133	1.137891	1.1246752	1.183634
b_2	6.003788	6.2246617	5.986011	6.002979	6.1044000	5.928038	5.950512	6.0555914	5.898785
c_2	1.570189	1.5553651	1.551328	0.892488	0.8333845	0.895651	1.598395	1.5243373	1.592000

TABLE 3: List of Distance-Dependent Scaling Factors

i, j	$\chi_{ij,small}^{ss}$	$\chi_{ij,large}^{ss}$	$\chi_{ij,small}^{sp}$	$\chi_{ij,large}^{sp}$	$\chi_{ij,small}^{pp}$	$\chi_{ij,large}^{pp}$	f_{ij}	r_{ij}^0
				Model 1				
O, H	0.714	0.722	1.163	0.989			0.875	1.287
C, H	1.645	1.358	0.909	0.972			1.094	1.090
C, O	0.903	1.296	1.217	1.635	0.721	1.321	1.208	1.040
C, C	0.791	0.903	1.083	1.863	1.426	1.010	0.813	1.108
H, H	0.697	0.806					1.518	1.429
				Model 2				
O, H	0.740	0.802	1.015	1.024			4.235	1.198
C, H	1.189	1.026	0.855	0.979			2.068	1.973
C, O	0.607	0.713	0.929	1.852	1.056	0.756	1.479	2.437
C, C	1.212	1.001	1.065	0.710	0.964	1.096	2.596	2.868
H, H	0.535	1.197					1.845	0.895

TABLE 4: Comparison between PM3-SRP Model 2 and ab Initio Energies

reaction	PM3-SRP model 2				ab initio			
	$\Delta E^\ddagger$	$\Delta E_{ZPE}^\ddagger$	ΔE^0	ΔE_{ZPE}^0	$\Delta E^\ddagger$	$\Delta E_{ZPE}^\ddagger$	ΔE^0	ΔE_{ZPE}^0
P1[a]	12.9	9.0	−12.6	−16.0	12.9	9.0	2.7	−1.4
P2	37.3	34.5	15.1	9.2	51.5	48.3	15.0	11.8
P3	53.3	51.3	−0.1	−5.7	50.2	46.9	6.3	1.1
S1	10.7	8.9	−17.0	−17.3	6.1	4.3	−16.6	−17.8
S2	9.9	7.9	−9.3	−10.4	6.2	4.9	−11.1	−10.2
S3	2.3	0.1	0.1	−3.7	16.0	14.5	3.6	1.2
S4	−0.7	−1.5	−5.6	−8.3	10.5	9.6	−4.5	−6.0
S5	11.6	6.8	−13.5	−12.0	13.8	13.3	−10.3	−9.2
UD1	20.4	16.5	5.2	0.1	16.5	14.4	11.2	5.3
UD2	13.0	9.1	19.8	14.2	29.5	24.7	13.0	6.4
UD3	16.9	15.1	15.8	11.3	24.0	21.8	17.3	12.4
UD4	24.3	22.3	10.1	6.5	11.8	9.8	2.9	−3.7
UD5	13.5	8.5	20.4	15.0	25.4	20.4	18.7	11.9
UD6	18.3	14.2	26.5	20.6	18.8	14.1	10.3	3.4

[a] Reactions P1, P3, S1, and S2 are calculated with MRCI+Q, extrapolated to the infinite basis set, see ref 16. The other reactions are calculated with PMP2/cc pVTZ//UMP2/cc-pVTZ. Energies are in kcal/mol.

The PM3-SRP model 2 and ab initio energetics are compared in Table 4. As described above, to develop this model all of the reactions in Figures 1 and 2 were fit except UD7 in Figure 2. The PM3 energetics are not listed in Table 2 to simplify the presentation. However, the inaccuracies in the PM3 energetics shown in Table 1 for the model 1 reactions are indicative of the inaccuracies in the PM3 energetics for the reactions in Table 4. Even though the energetics for the reparametrized PM3-SRP model 2 are much improved over the PM3 energerics, this model is not able to quantitatively reproduce the energies for all 14

reactions included in the fit. For example, there are substantial differences in the model 2 and ab initio barriers for the reactions P2, S3, S4, UD2, and UD5 and in the heat of reactions for UD4 and UD6. Even with reparametrization, the PM3 semiempirical method, which is based on a UHF wavefunction and a minimal basis set, has difficulty in reproducing the ab initio energies for reactions with open-shell radicals. The H atom is a reactant or product for P2, S3, S4, and UD5−UD7, and that the H atom has only a 1s-STO basis function might in part explain why the PM3-SRP model has difficulties in fitting the ab initio energetics for these reactions. For reactions S3 and S4, the PM3-SRP model 2 predicts loose TSs with essentially no barriers, in contrast to the tighter ab initio TSs with a barrier of 10−15 kcal/mol.

Even though there are at most only 14 reactions included in the above SRP fitting, this procedure is the most time-consuming step for the work presented here. Basically, it is difficult to satisfy all of the criteria in eq 10 because of the inherently approximate nature of semiempirical methods. It is possible that the SRP parameters and distance-dependent scaling factors determined here do not correspond to the fully optimized set of parameters. Even though the genetic algorithm is capable of searching for the global minimum, it is still very difficult to locate a global minimum of a hypersurface with 79 parameters that are optimized simultaneously. Therefore, refinement of the SRP fitting will continue, and updates of the parameters for a better description of the reactions studied here as well as a further extended library with more reactions are quite possible. The derived PM3-SRP potentials are most applicable to the reactions for which they are parametrized.

C. O(^{3}P)−Hydrocarbon van der Waals Potential. Collisions of O(^{3}P) with alkanes have long-range van der Waals interactions. When an O(^{3}P) atom collides with an alkane liquid, solid, or cluster, the low-frequency intermolecular modes of these alkane systems might efficiently absorb the atom's translational energy, causing the atom to become physisorbed, temporarily trapped in the O(^{3}P)−alkane potential energy minimum. This trapping will increase the time of the O(^{3}P) + alkane interaction and, thus, possibly enhance the likelihood that the O(^{3}P) atom abstracts a H atom or that the molecular system undergoes a transition from the triplet to singlet PES. Both are expected to enhance the O(^{3}P) processing of alkanes. The O(^{3}P) + C$_2$H$_6$ PM3-SRP potential developed here can be used in QM direct dynamics simulations of O(^{3}P) collisions with

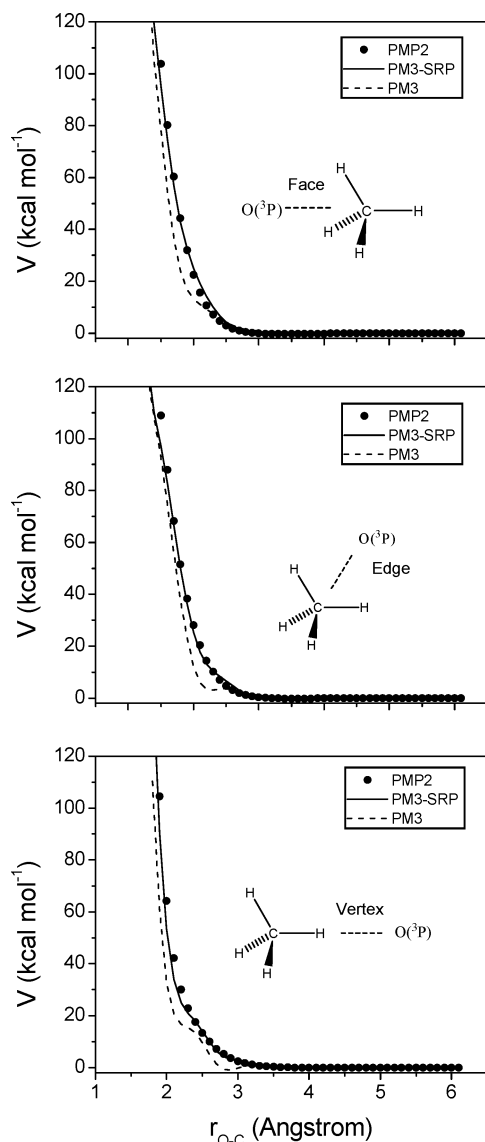**9868** *J. Phys. Chem. A, Vol. 108, No. 45, 2004*

Yan et al.

Figure 3. PM3-SRP + analytic functions, eqs 11−12, fit to PMP2// UMP2/cc-pVTZ potential energy curve for O(^{3}P) approaching CH$_4$ in three different configurations. The PM3-SRP is model 2. The PM3 curves are shown for comparison.

large alkane molecules and alkane clusters and can also be used to help "build" QM/MM models for O(^{3}P) collisions with alkane surfaces. Thus, it is important that the PM3-SRP model accurately represent the O(^{3}P)−alkane van der Waals interaction.

Here, the O(^{3}P) + CH$_4$ system is used to identify the van der Waals interaction between O(^{3}P) and alkanes. As shown in Figure 3, potential energy curves were calculated for O(^{3}P) interacting with the CH$_3$ *face* of CH$_4$ along the O···H$_3$CH C_{3v} axis, an *edge* of CH$_4$ and bisecting a H−C−H angle along a C_{2v} axis, and a *vertex* configuration along the O···HCH$_3$ C_{3v} axis. The UMP2 level of theory, with the aug-cc-pVTZ basis set[30] and with full counterpoise (CP) correction to account for basis set supersposition error (BSSE),[31] was used for the calculations. The final energy is further corrected with spin projection.[32−35] The PMP2//UMP2/aug-cc-pVTZ well depth is −0.27 kcal/mol at 3.4 Å for the face configuration, −0.18 at 3.6 Å for the edge configuration and −0.06 at 4.2−4.3 Å for the vertex configuration. A previous crossed-beam experiment on O(^{3}P)−CH$_4$ gave an average well depth of −0.22 kcal/mol at 3.57 Å.[36] Spin-projected MP2 with the aug-cc-pVTZ basis set gives an accurate intermolecular potential for this system.

TABLE 5: Parameters for the Analytic Function Representing O(^{3}P) + Alkane Long-Range Interactions

	a (kcal/mol)	b	c [(mol/kcal)/Å^6]	α	r_0 (Å)
O−C	11631.80	3.59	−427.46	23.87	2.63
O−H	7618.52	4.00	−117.90	28.94	3.00

Semiempirical theory, with only a minimal basis set, is well-known to describe long-range van der Waals interactions inaccurately. Therefore, we did not try to fit the long-range attraction between O(^{3}P) and C$_2$H$_6$ in developing the PM3-SRP models 1 and 2 described above. To develop a semiempirical model that has an accurate long-range interaction for O(^{3}P) colliding/reacting with an alkane, the above PM3-SRP model 2 is supplemented with an analytic function so that the total potential energy is

$$V = V_{\text{PM3−SRP}} + V_{\text{analytical}} \qquad (11)$$

The analytic component is a sum of O−H and O−C two-body terms, each a combination of Lennard-Jones $1/r^6$ and Buckingham functions. The parameters for the analytic component were determined by using this model to fit the O(^{3}P) + CH$_4$ potential energy curve in Figure 3. $V_{\text{analytical}}$ is written as

$$V_{\text{analytic}} = \sum_{\text{O−C,O−H}} S(r)[a \exp(-br) + c/r^6] \qquad (12)$$

where

$$S(r) = \frac{1}{2}\{1 + \tanh[\alpha(r - r_0)]\} \qquad (13)$$

is a switching function, which switches off the analytic contribution at short range. The O−H and O−C parameters for V_{analytic} are given in Table 5. The large α values means that the switching function in eq 13 is turned on/off suddenly. Also, the r_0 values are large enough to prevent this analytic correction for the long-range interaction from affecting any chemical reactivity. As shown in Figure 3, eqs 11−13 with these parameters give an excellent fit to PMP2 potential energy curves for O(^{3}P) + CH$_4$. The PMP2 energy and O−C distance for the potential minima in the "face" and "edge" potential energy curve are −0.27 kcal/mol, 3.4 Å, and −0.18 kcal/mol, 3.6 Å, respectively. For comparison, these values are −0.24 kcal/mol, 3.4 Å, and −0.28 kcal/mol, 3.6 Å, for the $V_{\text{PM3−SRP}} + V_{\text{analytic}}$ model.

III. Direct Dynamics Trajectory Simulation of O(^{3}P) + C$_6$H$_6$ Collisons and Reactions at 5 eV

A. Computational Procedure. With the increased speed of computers, it has become possible to use electronic structure theory directly in direct dynamics classical trajectory simulations.[37,38] The first direct dynamics simulation[39] used CNDO theory,[40,41] and semiempirical electronic structure theory remains an important method for direct dynamics simulations because it scales by O(N^2), is much faster than ab initio or DFT methods, and can be reparametrized to represent the chemical system of interest. Ab initio direct dynamics is often restricted to lower levels of theory and/or a relatively small basis set, giving rise to a potential energy surface that is only qualitatively accurate. A semiempirical theory, with fully optimized parameters, can describe the chemical reactivity as well as does high levels of theory and/or experiments. However, as described above, it is a challenge for a reparametrized semiempirical theory to accurately represent a system as complex as O(^{3}P) + C$_2$H$_6$ at high collision energy.

1. Computer Program and Trajectory Initial Conditions. The direct dynamics simulation was carried out by interfacing VENUS[42] with the semiempirical electronic structure package MOPAC7.0,[25] with the necessary modifications to include the distance-dependent scaling factors[26,27] and the analytic potential for the long-range interactions. The resulting package is called VENUS-MOPAC.[43] Quasiclassical normal-mode sampling[44,45] was used to sample a canonical ensemble of C_2H_6 molecules for the trajectories. The vibrational energy for each normal mode was sampled according to a 300 K Boltzmann distribution and, together with the ZPE, added to the normal mode with a random vibrational phase. The system so prepared, in normal-mode coordinates, is transformed to Cartesian coordinates. A rotational energy is added to each rotational degree of freedom according to a 300 K classical Boltzmann distribution. The initial separation between O(^{3}P) and the C_2H_6 center of mass (c.m.) is set to be 6 Å, with C_2H_6 randomly oriented. The impact parameter is sampled with $b = b_{max}(\xi)^{1/2}$, where b_{max} is chosen uniformly between 0 and 1. b_{max} is 3.5 Å, which is large enough to ensure there are no reactive events at larger b. Therefore, the impact region is sampled uniformly within a circle of 3.5 Å radius. The initial O(^{3}P) and C_2H_6 relative translational energy is fixed at 5 eV. The c.m. velocity of the whole system [O(^{3}P) + C_2H_6] is 0, and the system represents a c.m. frame, not a laboratory frame. The above procedures are standard options in the general chemical dynamics package VENUS.[42] A total of 50000 and 50107 trajectories were calculated for models 1 and 2, respectively, to have a detailed description of the complex O(^{3}P) + C_2H_6 reaction dynamics.

2. Integrating the Classical Equations of Motion. To calculate the classical trajectories, Hamilton's equations of motion are integrated by VENUS[42] with a combined fourth-order Runge−Kutta and sixth-order Adams−Moulton predictor−corrector algorithm.[46] The modified MOPAC[47] is called whenever potential energy and/or its derivatives are needed. There are two criteria for terminating a trajectory: (1) nonreactive trajectories are terminated when the center-of-mass separation between O(^{3}P) and C_2H_6 is larger than 7 Å after the collision's inner turning point in the O(^{3}P) and C_2H_6 relative motion, and (2) reactive trajectories are integrated up to 500 fs to monitor possible secondary reactions including the unimolecular dissociations in Figures 1 and 2.

To calculate the potential energy and its derivatives for the PM3-SRP model, the SCF convergence criterion is set to 10^{-4} kcal/mol for fast convergence. For each trajectory, a fresh guess of the density matrix is used for the first integration step, and the converged density matrix is then used for a good initial guess for the following integration steps. The integration time step is reduced to 0.1 fs for this fast collision (5 eV) system, and with this small time step, relatively few SCF iterations are needed to converge the density matrix. There are some trajectories that experience one or two convergence failures during the integration as O(^{3}P) approaches C_2H_6, particularly near a transition state structure.[28] When SCF failure occurs, a fresh guess of the density matrix is generated and a more sophisticated Camp−King converger,[48] one of the MOPAC 7.0 convergence options, is used; this often results in a converged density matrix, although it is slow. However, about 0.4% of the trajectories still experience SCF convergence failure after this second try and therefore are discarded. Another 0.2% of the trajectories do converge, but to a state different than the desired triplet, and are also discarded. Energy is conserved to within 1% of its initial value for most of the trajectories retained.

Ab initio/semiempirical quantum chemistry package are primarily for stationary-point calculations, i.e., searching for a TS or optimizing a structure, with the initial geometry often adjusted by hand using chemical intuition. For a direct dynamics simulations, the system can be driven by the equations of motion to severely distorted geometries where there are strong couplings between multiple PESs that makes SCF convergence difficult. There are some current developments underway for obtaining a good initial guess of the density matrix for this latter case,[49] and further development/implementation of a new SCF convergence algorithm for VENUS-MOPAC[43] is possible.

B. Trajectory Results. The O(^{3}P) + C_2H_6 reaction dynamics determined from the trajectory calculations for PM3-SRP models 1 and 2 are presented in the following subsections. The calculations were performed for a relative translational energy of 5 eV and C_2H_6 rotational/translational temperature of 300 K.

1. Individual Trajectories. The snapshots of four representative trajectories in Figure 4 illustrate some of the complex reaction dynamics of the O(^{3}P) + C_2H_6 collisions. The trajectory for channel 7 forms acetaldehyde and two H atoms as the reaction products. One H atom dissociates between 50 and 100 fs to form a short-lived ethoxy radical, which eliminates the second H atom at about 150 fs. According to the reactions in Figures 1 and 2, this trajectory is identified as a P2 → UD2 event. For the channel 11 trajectory, a H atom is ejected when O(^{3}P) and C_2H_6 collide, i.e., in the P2 channel. The energetic C_2H_5O radical then dissociates to CH_3 + formaldehyde between 180 and 200 fs to give a P2 → UD1 event.

The trajectories for channels 13 and 18 illustrate the difficulty in classifying some of the reactions in terms of a primary channel followed by secondary and unimolecular reactions. For the channel 13 trajectory, H_2 is formed at approximately 50 fs, leaving the triplet CH_3CHO radical, which dissociates to CH_3 and HCO between 200 and 250 fs. For the channel 18 trajectory, H_2 is also formed at about 50 fs, but triplet CH_3CHO first eliminates a H atom at about 90 fs and then dissociates to CH_3 and CO at about 200 fs. The formation of H_2 is the initial step for these two channels, with the two H atoms on the CH_3 group to which O(^{3}P) is added appearing to be squeezed together. We have denoted this as a P2 → S4 event, with the P2 and S4 steps occurring almost simultaneously. The channel 13 trajectory is then identified by the P2 → S4 → UD4 sequence of steps. The channel 18 trajectory has the same first two steps, with its next two steps not identified in Figure 2. The decomposition pathways observed for CH_3CO are the expected Norrish type I cleavage pathways of a triplet aldehyde.

2. Opacity Functions. Opacity functions, probabilities of reaction versus impact parameter b, for both models 1 and 2 are shown in Figure 5 for several product channels. Overall, there is very good agreement between the opacity functions for the two models. For model 1, opacity functions are given that combine channels 11 and 13 and channels 12 and 14. However, because channels 11 and 13 dominate these opacity functions, they can be compared with the model 2 opacity functions for channels 11 and 13. The only substantial difference in the results for the two models is for channel 18, whose reaction probability is much larger for model 2. Both models show that the reaction probabilities for channels 11 and 13 increase as the impact parameter approaches zero. For channels 1, 7, and 8, the opacity function peaks at intermediate parameters, with the peak at ~2 Å for channel 1 and at smaller values of b for the other two channels. Similar opacity functions for multiple product channels is a marker that these channels might occur by the same type of reaction dynamics. The peaking in the opacity function for
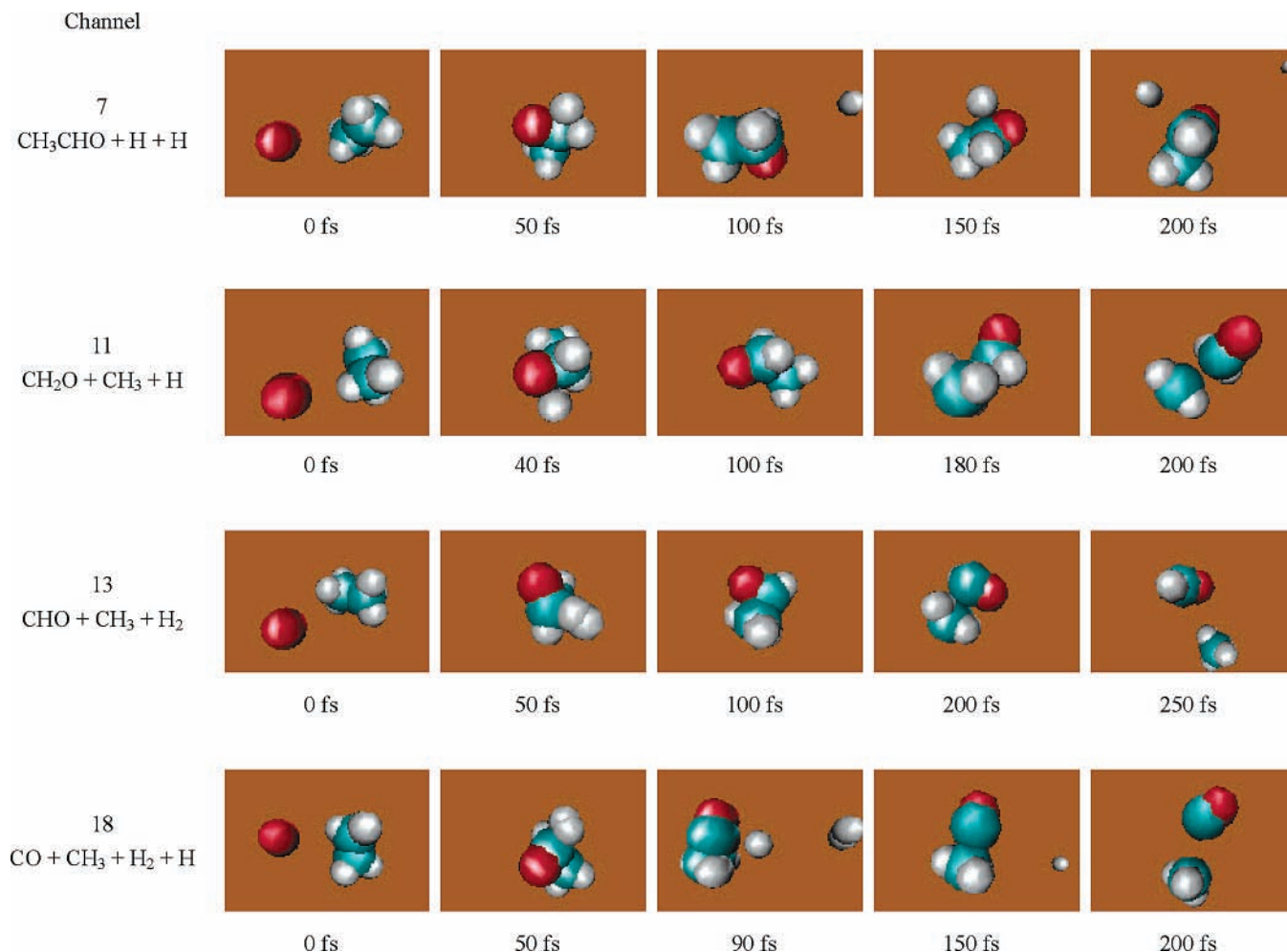
Channel

Figure 4. Snapshots of four $O(^3P) + C_2H_6$ reactive trajectories giving the products for channels 7, 11, 13, and 18. The trajectories were calculated with model 2.

channel 1, OH formation, at a large value of *b* suggests it occurs by a "stripping" mechanism. This is the only important reaction that occurs at impact parameters larger than 2.1 Å. There are no reactive trajectories at impact parameters larger than about 3.2 Å.

The opacity function for channel 1, as a function of the vibrational state of the OH product, is given in Figure 6. There is a tendency for the opacity function to flatten and broaden and for its peak move to a larger *b* as the vibrational level increases. The relative population of the 0, 1, and 2 vibrational states is 1:0.80:0.38.

3. Reactive Cross Sections. Cross sections for the different product channel are listed in Table 6. Statistical uncertainties are not included, because with more than 50000 trajectories for each model, the uncertainties are quite small. A substantial amount of the 5 eV high collision energy is deposited into the methoxy, CH_3O, and ethoxy, C_2H_5O, products of channels 3 and 2, and as a result, these primary products undergo secondary unimolecular reactions. This leads to large numbers of reaction products and small cross sections for channels 2 and 3. Because channel 1 occurs by a stripping mechanism as shown in Figure 5, only a small fraction of the 5 eV collision energy is deposited in its C_2H_5 product. Little dissociation of C_2H_5 to $H + C_2H_4$ occurs, as shown by the large cross section for channel 1 and the much smaller cross section for channel 4. Because of the importance of unimolecular dissociation for the products of primary channels 2 and 3, the cross sections calculated from the trajectories strongly depend on the length of time the

trajectories are integrated. Clearly, as shown by the trajectory snapshots in Figure 4, fewer product channels would have been observed if the trajectories were integrated for only 100 ps instead of the 500 ps calculated here. Indeed, the trajectory cross sections might change and additional products might be formed if the trajectories were integrated for an even longer time. Some of the products observed at 500 ps might have sufficient energy to unimolecularly dissociate on a longer time scale.

There are important relationships between the many product channels presented in Table 6. For channels 5 and 6, as the OH radical departs, it "grabs" another H atom. The resulting H_2O formation is dynamically controlled, as the two abstracted H atoms tend to come from the same methyl group; i.e., the cross section for channel 6 is an order of magnitude larger than that for channel 5. This result was also observed by Schatz and co-workers.[14] The CH_3O methoxy radical of channel 3 can dissociate to H and H_2CO, forming channel 11, and possibly also to $H_2 + HCO$, forming channel 13. The energies for this latter channel were not investigated in the ab initio calculations presented in secion II.A.[50] If HCO retains sufficient internal energy, it will dissociate to H + CO, yielding channel 18. The CH_3 and CH_3O products of channel 3 can undergo a secondary reaction, forming CH_4 and triplet CH_2O, which will dissociate to H + HCO, yielding channel 14. If HCO then dissociates to H + CO, the products of channel 20 are formed. Thus, channels 11, 13, 18, 14, and 20 might originate from primary channel 3.

Quite a large number of reactions are promoted by primary channel 2. The vibrationally excited C_2H_5O radical product can

PES Model for O(^{3}P) Reactions with Alkanes

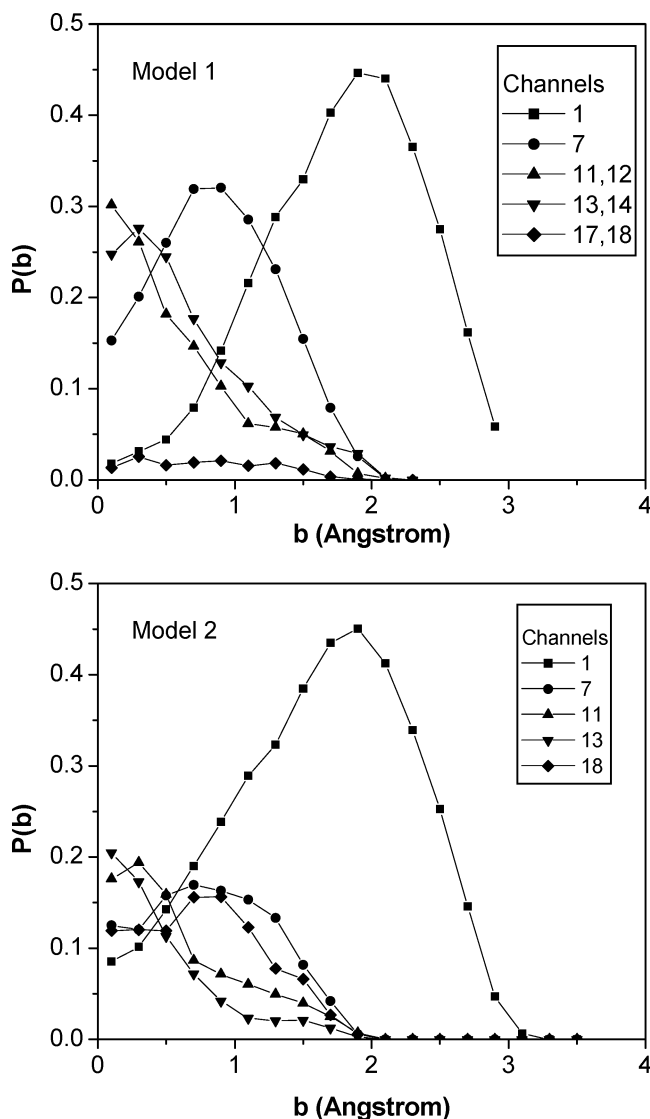*J. Phys. Chem. A, Vol. 108, No. 45, 2004* **9871**

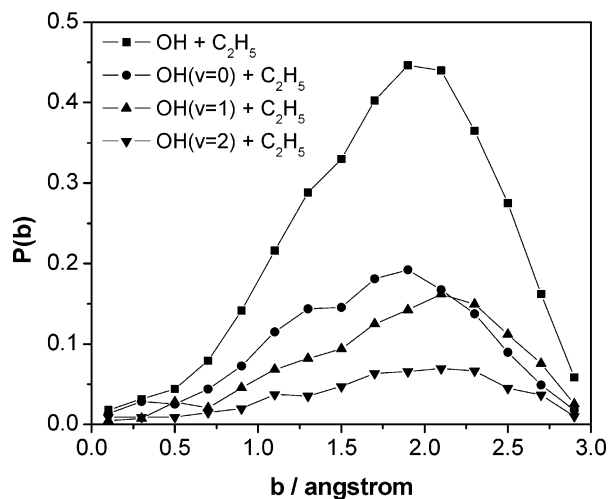**Figure 5.** Opacity functions for five of the product channels calculated with models 1 and 2.

Figure 6. Opacity function for channel 1 as a function of the OH vibrational state. Calculations are for model 1.

dissociate either a H atom or CH_3 radical, forming acetaldehyde or formaldehyde, respectively, for channels 7 or 11. For channel 8, acetaldehyde is in its cyclic ethylene oxide (i.e., oxirane) isomeric structure. The ethoxy radical has isomerized to its enol
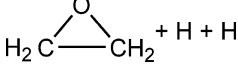
structure in channel 21. Even though the total heat of reaction for each of these channels is highly endothermic (63.7 and 51.5 kcal/mol with PM3-SRP model 2), the 5 eV collision supplies sufficient energy as long as it is efficiently transferred to internal energy of the ethoxy radical.

The H atom product from channel 2 can undergo a secondary reaction, abstracting a H atom to form H_2 and the triplet radicals in channels 9, 10, and 22. For channels 9 and 10, the two H atoms forming H_2 come from different and the same carbon atoms, respectively, while the triplet radical in channel 22 is an isomer of those in channels 9 and 10. Because of the low barriers for unimolecular decomposition of these triplet radicals, the cross sections for their formation are small. The relative importance of channels 9 and 10 can be established from the cross sections for products that originate from these two channels. The triplet radical in channel 9 dissociates to CH_2O and $^3CH_2$ to give the products in channel 12. The triplet radical in channel 10 dissociates either to the CH_3 + HCO products in channel 13 or to H and CH_3CO, with the latter possibly dissociating to give the CH_3 + CO products in channel 18. Similarly, the HCO product of channel 13 can dissociate to H + CO, forming the channel 18 products. Thus, both channels 13 and 18 can follow channel 10. Regardless of the importance of channel 18 in this sequence, the fact that the cross section for channel 13 is an order of magnitude larger than that for channel 12 shows that channel 10 is much more important than channel 9. The dominance of channel 10 shows that the two H atoms eliminated from C_2H_5O to form H_2 tend to come from the same carbon atom in a manner similar to how H_2O is formed.

The above discussion shows that channels 7−13, 18, 21, and 22 might originate from primary channel 2. Given the channels associated with primary channels 1 and 3, the only channels that have not been related to a primary channel are channels 15−17 and 19. Channel 15 might follow channel 20, when the CH_2CHOH triplet radical dissociates to CH_2CHO + H. Channel 16 might be an additional step in this sequence, with CH_2CHO dissociating to CH_2CO (ketene) + H. A possible precursor for channel 17, and formation of triplet ketene, is the elimination of H_2 from the triplet radical products in channels 9, 10, and 22. One possible pathway for channel 19 is dissociation of triplet ketene in channel 17. It should be recognized that these are only conjectures concerning the sequence of reactions leading to product channels 15−17 and 19. However, given the nature of the products for these channels, it seems likely that they are initiated by primary channel 2.

To compare models 1 and 2 and to compare the relative importance of primary channels 1−3 (P1−P3), it is useful to sum the cross sections for the product channels associated with each primary channel. Some of the product channels are associated with both P2 and P3, with one-half of the cross sections for these channels is contributed to both P2 and P3. The product channels 1 and 4−6 are associated with P1; channels 2, 7−10, 11 ($^1/_2$), 12, 13 ($^1/_2$), 15−17, 18 ($^1/_2$), 19, 21, and 22 are associated with P2; and channels 3, 11 ($^1/_2$), 13 ($^1/_2$), 14, 18 ($^1/_2$), and 20 associated with P3. Using this analysis, the model 1 primary cross sections for P1−P3, before any ensuing events, are estimated as 7.56, 3.71, and 1.15 Å^2, and those for model 2 as 7.97, 2.65, and 1.10 Å^2, respectivelt. These sets of cross sections are in good agreement. Channel 1 is the most important primary channel, consistent with the previous simulation of this system by Schatz and co-workers.[14] In comparing the model 1 and model 2 cross sections in Table 6 for the different product channels, one sees that decomposition of the ethoxy product of channel 2 is less important for model

TABLE 6: Reaction Cross Sections of Different Channels

| | | | cross section[c] | |
channel	products[a]	proposed reaction path[b]	model 1	model 2
1	OH + C$_2$H$_5$	P1	7.14	7.76
2	C$_2$H$_5$O + H	P2	0.30	0.009
3	CH$_3$O + CH$_3$	P3	0.025	0.014
4	OH + H$_2$C=CH$_2$ + H	P1 → UD7	0.082	0.046
5	H$_2$O + H$_2$C−CH$_2$	P1 → S1	0.031	0.019
6	H$_2$O + CH$_3$CH	P1 → S2	0.31	0.14
7	CH$_3$CHO + H + H	P2 → UD2	2.06	1.17
8	(epoxide: H$_2$C—O—CH$_2$) + H + H	P2 → UD2 → isom[d]	0.13	0.057
9	CH$_2$CH$_2$O + H$_2$	P2 → S3	0.021	<0.001
10	CH$_3$CH−O + H$_2$	P2 → S4	0.087	<0.001
11	CH$_2$O + CH$_3$ + H	P2 → UD1 → P3 → UD5	0.80	0.65
12	CH$_2$O + CH$_2$ + H$_2$	P2 → S3 → UD3	0.026	0.042
13	CHO + CH$_3$ + H$_2$	P2 → S4 → UD4	0.77	0.41
14	CHO + CH$_4$ + H	P3 → S5 → UD6	0.27	0.071
15	CH$_2$CHO + H$_2$ + H			0.20
16	CH$_2$=C=O + H$_2$ + H + H		0.060	0.072
17	C$_2$H$_2$O + H$_2$ + H$_2$		0.17	0.007
18	CO + CH$_3$ + H$_2$ + H		0.14	0.93
19	CO + CH$_2$ + H$_2$ + H$_2$			0.084
20	CO + CH$_4$ + H + H			0.016
21	CH$_3$CHOH + H	P2 → isom		0.061
22	CH$_2$CHOH + H$_2$	P2 → S3 → isom		0.014

[a] Products are on the ground-state triplet potential energy surface. [b] Nomenclature for the proposed reaction paths is defined in Figures 1 and 2. [c] Cross sections are in units of Å^2. [d] Isom means the product isomerizes.

1 than for model 2, giving rise to a much larger cross section for this channel with model 1. Also, the cross section for channel 18, which follows channel 13, is much larger for model 2. It is worth noting that the sums of the cross sections for channels 13 and 18 are 0.91 and 1.34 Å^2, respectively, for models 1 and 2 and not that different. Overall, models 1 and 2 give similar patterns in the cross sections for the different product channels.

In concluding this section, we need to point out a shortcoming of the PM3-SRP parameters. As shown in Table 4, model 2 predicts essentially no barriers for the secondary reactions S3 and S4, whereas the ab initio barriers are 10−15 kcal/mol. As a result, H$_2$ formation via these channels is expected to be artificially high. Channel 18 is significant for model 2, and a route to this channel is through channel 10, which occurs by the P2 → S4 step. The triplet aldehyde in channel 10 can decompose to give CH$_3$ + H + CO sequentially or nearly simultaneously. The result is that model 2 predicts a significant amount of CO, that might be too large as a result of a too-high probability of H$_2$ formation. Thus, the validity of the proposed CO formation needs to be examined by experiment. However, for 5 eV collision of O(^{3}P) with C$_2$H$_6$, CO is a likely product. In a recent experimental study of the O(^{3}P) + C$_2$H$_5$ reaction by time-resolved Fourier transform infrared emission spectroscopy, CO was observed as a product.[51] The trajectories calculated here predict the formation of formaldehyde, by decomposition of the ethoxy radical in path P2 to CH$_3$ + H$_2$CO or decomposition of the methoxy radical in path P3 to H + H$_2$CO. The former was previously proposed by Vivier-Bunge and co-workers.[52]

4. Angular Distributions. Product scattering angles within the c.m. frame are often measured for A + B → C + D reactions.[53] A crossed-beam experiment usually measures just one of the products, and the other is completely determined because the c.m. motion remains constant. A laboratory-to-c.m. transformation[54] is then applied to determine the scattering angles in the c.m. frame. For the direct dynamics simulation carried out here, there are up to three or four fragments for some of the channels, i.e., the prototype reactions A + B → C + D + E and A + B
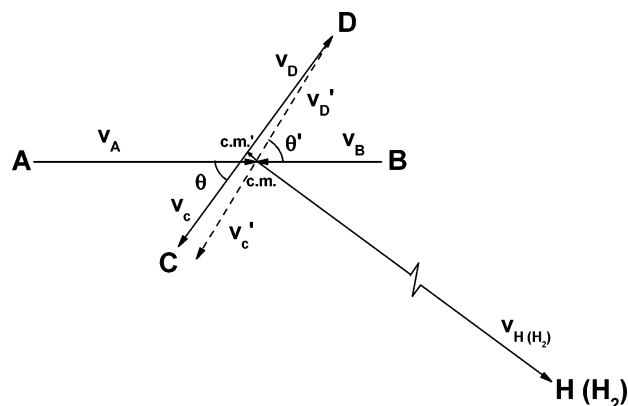

Figure 7. Velocity vector diagram of A + B → C + D + H (or H$_2$) prototype reaction in the c.m. frame. If H (or H$_2$) is much lighter than C and D, the real deflection angle θ can be well-represented by angle θ' (A + B → C + D prototype reaction) by neglecting H (or H$_2$).

→ C + D + E + F. Although the scattering angle can be calculated from the trajectory without ambiguity, an additional assumption is necessary to measure the scattering angle experimentally. Because the channels with three or four products involve H atom(s) and/or H$_2$ molecule(s), a valid assumption is that, because they are light, they do not significantly affect the motion of the heavier products. This kinematics is illustrated in Figure 7 for a prototype reaction A + B → C + D + H (or H$_2$), where the center of mass (c.m.′) of the products C + D can be approximated to reside on the center of mass (c.m.) of the whole system. By such an approximation, the reaction is reduced to the conventional A + B → C + D reaction. The deflection angle θ' for the above approximation can be measured experimentally. The real deflection angle is denoted as θ in Figure 7. With a computer simulation, one can calculate both θ and θ' to examine the accuracy of this approximation. Because the products of the primary channels P2 and P3 can undergo significant secondary and unimolecular dissociation reactions, the experimental scattering angles for these channels do not reveal the nascent scattering dynamics, before the secondary
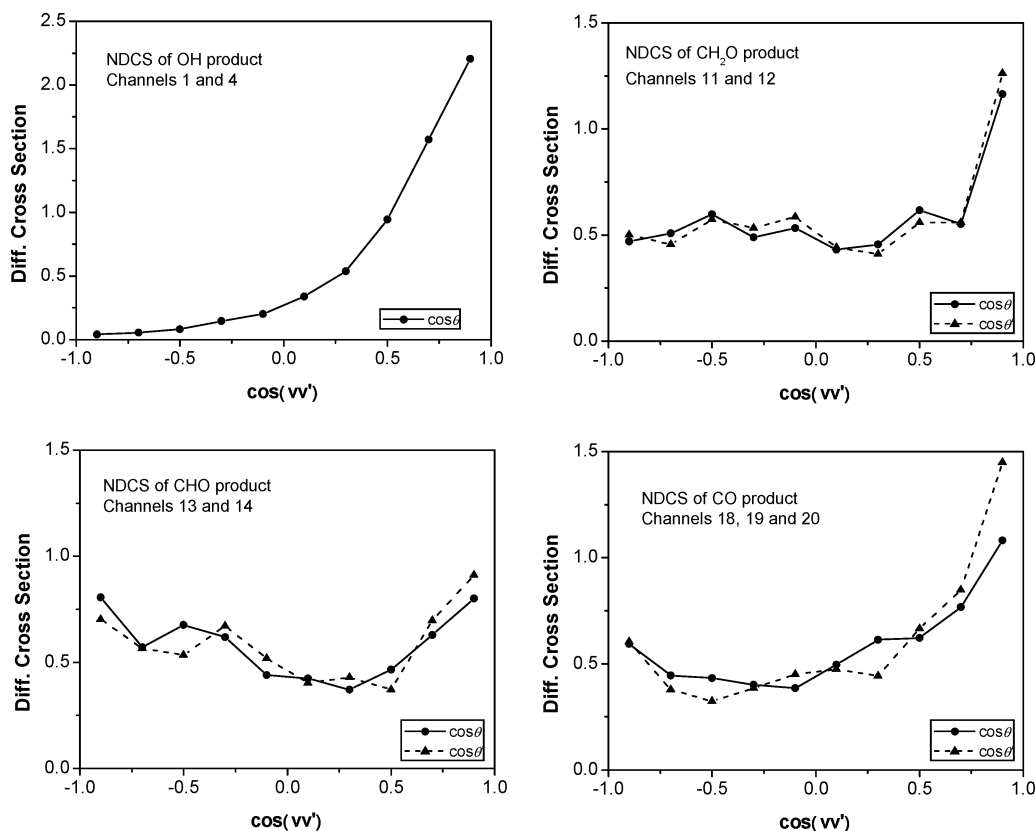
PES Model for O(^{3}P) Reactions with Alkanes

J. Phys. Chem. A, Vol. 108, No. 45, 2004 **9873**

Figure 8. Normalized differential cross sections, $(1/\sigma)[\Delta\sigma/\Delta(\cos\theta)]$, for different channels (see Table 6). $\Delta(\cos\theta) = 0.2$ for the curves. The results are based on model 2.

and dissociation reactions. Thus, probing the scattering dynamics of the nonprimary channels is of considerable importance, and it is necessary to test the above approximate approach for determining their scattering angles.

Figure 8 shows the normalized differential cross sections (NDCSs) of several channels with OH, CH$_2$O, CHO, and CO as products, determined from the model 2 trajectories. Even though acetaldehyde is found to be the second most important product in this study, its NDCS is not calculated because it will primarily move with the c.m. motion by eliminating two light H atoms and a crossed-beam experimental measurement in the laboratory frame would detect most of them at the c.m. scattering angle. This makes it difficult to draw a dynamical picture for this channel. For the same reason, the NDCS of channel 2, with C$_2$H$_5$O as a product, is not calculated. Also there are very few trajectories for this channel, because most of the C$_2$H$_5$O radicals decompose as discussed above. The NDCS of channel 3, with CH$_3$O as product, is also not calculated because its reaction cross section is very small, with only 18 trajectories forming this product.

The NDCS for channels 1 and 4, with OH as a product, is shown in Figure 8. There is almost no ambiguity in the scattering angle for this channel using the conventional prototype A + B → C + D reaction, because channel 4 contributes an insignificant amount of OH. The angular distribution of OH is mostly forward scattered, the same as Schatz and co-workers[14] found. The forward scattering is consistent with a stripping mechanism. Channel 4 is mainly associated with small impact parameters that primarily fall in the range of 0.6−1.2 Å. These collisions, which have a low probability, deposit sufficient energy in the C$_2$H$_5$ product of P1 that it can dissociate to H + C$_2$H$_4$.

The angular distribution for the CH$_2$O product of channel 11 and 12 is shown in Figure 8. The scattering angles θ and θ' are

defined in Figure 7. The NDCS of the actual scattering is plotted by the solid line (cos θ), and the scattering angle determined by ignoring the light H atom is plotted by the dashed line (cos θ'). The similarity of the two curves illustrates the validity of the assumption of neglecting the light product. There are several important features in this angular distribution: (1) the strong forward scattering indicates a mechanism in which O(^{3}P) abstracts one of the methyl groups from C$_2$H$_6$ to form a forward-scattered CH$_3$O analogous to H-abstraction, as previously discussed by Schatz and co-workers.[14] The energetic CH$_3$O radical then eliminates a H atom to form formaldehyde, and (2) the flat region with a cos θ value less than 0.6 and the minimum in the scattering probability near 90° are indicative of a long-lived collision complex.

Figure 8 shows the NDCS for channels 13 and 14, with the HCO radical as the product. The curve for the actual scattering is given by the solid line, and the curve from ignoring the H$_2$ molecule or H atom is given by the dashed line. For these two channels, the NDCS is quite symmetric, indicating a long-lived collision complex prior to formation of HCO. Also given in Figure 8 is the NDCS for CO, a product of channels 18−20. These channels are four-product systems (see Table 6) with double H atom(s) and/or H$_2$ molecule(s) eliminations. As a consequence, the difference between the actual scattering angle θ and the approximate scattering angle θ' is large in comparison to the differences for the other plots in Figure 8. Except for the forward scattering component in the distribution, the NDCS for CO is more symmetric than are the NDCSs for the other products in Figure 8, suggesting that CO might be formed through a longer-lived intermediate (or intermediates) as compared to those for the other products. The forward scattering asymmetry suggests that some of the CO products are formed directly or through a very short-lived collision complex.

IV. Comparison with Previous Crossed-Beam Experiments and Direct Dynamics Simulations

Minton and co-workers have studied the $O(^3P) + C_2H_6$ reaction in crossed beams at a collision energy of 3.5 eV. They identified the primary channels P1−P3, leading to OH + C_2H_5, C_2H_5O + H, and CH_3O + CH_3, respectively, in their experiments. The same primary channels are observed in our simulations. However, they did not observe the large number of additional product channels, arising from secondary and unimolecular dissociation reactions of the primary channels' products, as found in our simulations. These secondary and unimolecular reactions become more important as the collision energy is increased, and the fact that our simulation is performed at energy 1.5 eV higher than that for the experiments is expected to be an important factor in understanding differences between the experiments and our simulations. It is also possible that higher resolution in the experimental measurements might reveal more products.

Minton and co-workers[55] investigated the decomposition of the OCH_3 radical in a crossed-beam study of the $O(^3P) + CH_4 \rightarrow H + OCH_3$ reaction at a collision energy of 2.9 eV. Because the reaction endothermicity is 0.62 eV, the energy available to the reaction products is 2.3 eV = 52.6 kcal/mol. MSINDO direct dynamics simulations of this reaction by Troya et al.[15] give 0.40 as the fraction of the available energy partitioned to OCH_3 internal energy. Thus, for this experiment, the internal energy of the OCH_3 product is estimated as 21 kcal/mol and lower than the 33 kcal/mol determined (see below) for this product in the simulations reported here of $O(^3P) + C_2H_6 \rightarrow CH_3 + OCH_3$. Minton and co-workers concluded that a significant fraction of their OCH_3 product dissociates to H + H_2CO and a small fraction isomerizes to CH_2OH, with a relative H_2CO/OCH_3/CH_2OH product yield of 0.73:0.22:0.05. Minton and co-workers' observation of less OCH_3 decomposition and fewer decomposition products, as compared to the results of the simulations reported here, is consistent with the lower OCH_3 internal energy in their experiments.

Troya et al. performed[14] a semiempirical MSINDO direct dynamics simulation to study the $O(^3P) + C_2H_6$ reaction at collision energies ranging from 0.65 to 5.75 eV. Their calculations at 3.92 and 5.75 eV bracket the simulations reported here for 5 eV and can be interpolated to compare with the current results. In comparison to our trajectories, which were integrated for 500 fs, Troya et al. integrated their trajectories for a much shorter period of time.[56] They observed the primary channels OH + C_2H_5, C_2H_5O + H, and CH_3O + CH_3 with interpolated cross sections at 5 eV of 5.32, 3.53, and 1.06 Å[2], respectively. The cross sections from our simulations are in overall good agreement with these values. The model 1 and 2 cross sections for channel 1 are 7.56 and 7.97 Å[2] and somewhat larger than the MSINDO cross section. This difference with MSINDO is similar to the difference observed between PM3 and MSINDO for the $O(^3P) + CH_4 \rightarrow OH + CH_3$ cross section,[15] which suggests that the PM3-SRP models retain the characteristic of giving a cross section larger than MSINDO for O(3P) + RH $\rightarrow$ OH + R abstraction. The model 1 and 2 cross sections for channel 3, of 1.15 and 1.10 Å[2], are in excellent agreement with the Troya et al. value of 1.06 Å[2]. During the short time of Troya et al.'s trajectory simulations, three additional product channels were observed, i.e., channels 5−7 forming H_2O + C_2H_4, H_2O + CH_3CH, and CH_3CHO + 2H. The cross section for channel 6 is much larger than that for channel 5, which is the same as found from models 1 and 2. The cross section interpolated to 5 eV for channels 5 + 6 and channel 7 are 0.56 and 0.056 Å[2],
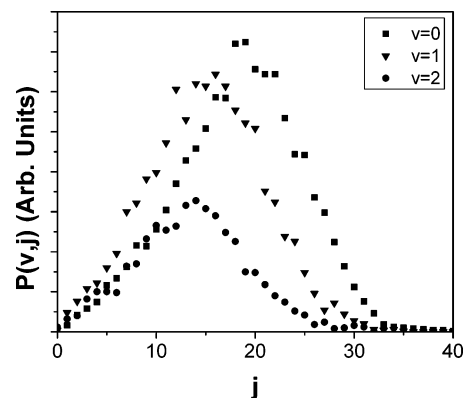

Figure 9. Vibrational and rotational energy distributions for the OH products of channel 1.

respectively. Troya et al.'s cross section for channel 7 is substantially smaller than the values of 2.06 and 1.17 Å[2] for models 1 and 2, respectively, but their value would be expected to increase if their trajectories were integrated for a longer period of time, allowing more dissociation of C_2H_5O.

Energy partitioning to reaction products other than OH was not determined in our simulations. However, Troya et al. analyzed the product energy partitioning for the primary product channels, and their results at 3.92 and 5.75 eV can be used to estimate the energy partitioning at 5 eV. For the OH + C_2H_5 products, the average partitioning is estimated to be 0.74 to translation, 0.16 to C_2H_5 internal, and 0.10 to OH rotation and vibration. For the H + C_2H_5O products, the energy partitioning is estimated as 0.36 to translation and 0.64 to C_2H_5O internal energy. For the CH_3O + CH_3 products, the estimated energy partitioning is 0.71 to translation, 0.29 to CH_3O internal energy, and 0.00 to CH_3 internal energy. Deposition of large amounts of energy into the C_2H_5O and CH_3O radical products is consistent with the extensive dissociation we observe for these products. The average internal energy available to the C_2H_5O product is the 5 eV collision energy minus the 11.8 kcal/mol reaction endothermicity for channel 2 (see Figure 1) multiplied by the 0.64 average fraction partitioned to C_2H_5O, which equals 66 kcal/mol. As shown in Figure 2, this average energy is in large excess of that required for C_2H_5O unimolecular dissociation. The 33 kcal/mol average internal energy of the CH_3O product is also in excess of that required for dissociation. The energy partitioning to the C_2H_5O and CH_3O products of the primary channels indicates that they will undergo extensive unimolecular decomposition as seen in our simulations.

Finally, the rotational and vibrational energy distributions found by Troya et al. for the OH product of channel 1 are similar to the results of our simulations, which are shown in Figure 9. They performed their analyses for a collision energy of 0.65 eV and found that the rotational distribution peaked at $j = 15$. We find at a collision energy of 5 eV that the peak is slightly dependent on the OH vibrational state v and is at j levels of 18, 15, and 14 for v levels of 0, 1, and 2, respectively. The relative population of the OH $v = 0/v = 1/v = 2$ state is 1.00:0.80:0.38. Troya et al.'s relative population is 1.00:0.53:0.063, which has more $v = 0$ and less $v = 2$ as compared to our results. This is consistent with their lower collision energy.

V. Summary

The work presented here includes PMP2/cc-pVTZ//UMP2/cc-pVTZ calculations of stationary-point energies, structures, and vibrational frequencies for a set of 14 reactions that participate in the reaction dynamics of high-energy $O(^3P)$ +

C_2H_6 collisions. This information and additional MRCI results, published previously[16] for reactions participating in the O(^{3}P) + C_2H_6 dynamics, were used to reparametrize PM3 semi-empirical electronic structure theory. Two PM3-SRP models, models 1 and 2, were derived by using different groups of reactions to fit the SRPs. Even though these two PM3-SRP models are unable to quantitatively represent all of the reactions that occur in high-energy O(^{3}P) + C_2H_6 collisions, they are vast improvement over the PM3 model.

These two PM3-SRP models are used in direct dynamics classical trajectory simulations of the O(^{3}P) + C_2H_6 reaction at a 5 eV collision energy. The two models give similar reaction dynamics, which are in overall good agreement with previous experiments by Minton and co-workers[17] and MSINDO direct dynamics trajectory simulations by Schatz and co-workers.[14] At this high collision energy, the O(^{3}P) + C_2H_6 reaction occurs via three primary channels yielding OH + C_2H_5, H + C_2H_5O, and CH_3 + CH_3O. The products of these primary reactions can undergo secondary reactions by colliding with each other, forming H_2O and triplet C_2H_4 and/or CH_3CH, H_2, and triplet CH_2CH_2O and/or CH_3CHO, CH_4, and triplet CH_2O. In addition, the alkoxy C_2H_5O and CH_3O products of the primary channels are highly vibrationally excited and can undergo unimolecular decomposition by multiple pathways forming a variety of products; e.g., C_2H_5O can dissociate to H + CH_3CHO (acetaldehyde), CH_3 + CH_2O (formaldehyde), H_2 + CH_3CO, or CH_4 + HCO. The radical products for the latter two channels can decompose to form CO, which has been observed as a product in an experimental study[51] of the O(^{3}P) + C_2H_5 reaction. Formaldehyde has previously been proposed[52] as a product in the unimolecular decomposition of the ethoxy radical C_2H_5O.

This work illustrates the challenges in using a semiempirical electronic structure theory as a functional to fit the results of high-level ab initio calculations for a complex chemical system. When reparametrized with specific reaction parameters (SRPs), PM3 is unable to quantitatively fit properties of the many reactions that participate in O(^{3}P) + C_2H_6 chemical dynamics. However, reparametrizing a semiempirical theory to represent a complex chemical system remains a useful strategy worth pursuing. More understanding is needed to identify the best semiempirical theoretical model to use for the reparametrization.

References and Notes

(1) Andresen, P.; Luntz, A. C. *J. Chem. Phys.* **1980**, *72*, 5842.

(2) Miyoshi, A.; Tsuchiya, K.; Yamauchi, N.; Matsui, H. *J. Phys. Chem.* **1994**, *98*, 11452.

(3) Tsurumaki, H.; Fujimura, Y.; Kajimoto, O. *J. Chem. Phys.* **2000**, *112*, 8338.

(4) Liston, E. M.; Martinu, L.; Wertheimer, M. R. *J. Adhes. Sci. Technol.* **1993**, *7*, 1091.

(5) Ellison, G. B.; Tuck, A. F.; Vaida, V. *Geophys. Res.* **1999**, *104*, 11633.

(6) Garton, D. J.; Minton, T. K.; Alagia, M.; Balucani, N.; Casavecchia, P.; Volpi, G. G. *Faraday Discuss. Chem. Soc.* **1997**, *108*, 387.

(7) Kelso, H.; Kohler, S. P. K.; Henderson, D. A.; McKendrick, K. G. *J. Chem. Phys.* **2003**, *119*, 9985.

(8) Li, G.; Bosio, S. B. M.; Hase, W. L. *J. Mol. Struct.* **2000**, *556*, 43.

(9) Minton, T. K.; Garton, D. J. In *Chemical Dynamics in Extreme Environments*; Dressler, R. A., Ed.; World Scientific: Singapore, 2001; p 420.

(10) Garton, D. J.; Minton, T. K.; Alagia, M.; Balucani, K.; Casavecchia, P.; Volpi, G. G. *J. Chem. Phys.* **2000**, *112*, 5975.

(11) Garton, D. J.; Minton, T. K.; Alagia, M.; Balucani, K.; Casavecchia, P.; Volpi, G. G. *J. Chem. Phys.* **2001**, *114*, 5958.

(12) Zhang, J.; Garton, D. J.; Minton, T. K. *J. Chem. Phys.* **2002**, *117*, 6239.

(13) Gindulyte, A.; Massa, L.; Bands, B. A.; Rutledge, S. K. *J. Phys. Chem. A* **2000**, *104*, 9976.

(14) Troya, D.; Pascual, R. Z.; Garton, D. J.; Minton, T. K.; Schatz, G. C. *J. Phys. Chem. A* **2003**, *107*, 7161.

(15) Troya, D.; Pascual, R. Z.; Schatz, G. C. *J. Phys. Chem. A* **2003**, *107*, 10497.

(16) Yan, T.; Hase, W. L.; Doubleday, C. *J. Chem. Phys.* **2004**, *120*, 9253.

(17) Garton, D. J.; Minton, T. K.; Troya, D.; Pascual, R.; Schatz, G. C. *J. Phys. Chem. A* **2003**, *107*, 4583.

(18) Troya, D.; Schatz, G. C. In *Materials in a Space Environment*; Special Publication SP-540; European Space Agency: Paris, 2003; p 121.

(19) Troya, D.; Schatz, G. C. *J. Chem. Phys.* **2004**, *120*, 7696.

(20) Langhoff, S. R.; Davidson, E. R. *Int. J. Quantum Chem.* **1974**, *8*, 61.

(21) Stewart, J. J. P. *J. Comput. Chem.* **1989**, *10*, 209.

(22) Stewart, J. J. P. *J. Comput. Chem.* **1990**, *11*, 543.

(23) Gonzalez-Lafont, A.; Truong, T. N.; Truhlar, D. G. *J. Phys. Chem.* **1991**, *95*, 4618.

(24) Chuang, Y.; Corchado, J. C.; Truhlar, D. G. *J. Phys. Chem. A* **1999**, *103*, 1140.

(25) Stewart, J. J. P. *MOPAC 7.0, A General Molecular Orbital Package*; QCPE: Bloomington, IN, 1993; Program 455.

(26) Doubleday, C.; Nendel, M.; Houk, K. N.; Thweatt, D.; Page, M. *J. Am. Chem. Soc.* **1999**, *121*, 4720.

(27) Doubleday, C. *J. Phys. Chem. A* **2001**, *105*, 6333.

(28) Stewart, J. J. P. In *Reviews in Computational Chemistry*; Lipkowitz, K. B., Boyd, D. B., Eds.; Wiley: New York, 1990; pp 45−82.

(29) Carroll, D. A. http://cuaerospace.com/carroll/ga.html.

(30) Dunning, T. H. *J. Phys. Chem.* **1989**, *90*, 1007.

(31) Boys, S. F.; Bernardi, F. *Mol. Phys.* **1970**, *19*, 553.

(32) Sosa, C.; Schlegel, H. B. *Int. J. Quantum Chem.* **1986**, *29*, 1001.

(33) Sosa, C.; Schlegel, H. B. *Int. J. Quantum Chem.* **1987**, *30*, 155.

(34) Sosa, C.; Schlegel, H. B. *Int. J. Quantum Chem. Symp.* **1987**, *21*, 267.

(35) Gonzalez, C.; Sosa, C.; Schlegel, H. B. *J. Phys. Chem.* **1989**, *93*, 2435.

(36) Liuti, G.; Pirani, F. *J. Chem. Phys.* **1987**, *87*, 5366.

(37) Sun, L.; Hase, W. L. In *Reviews in Computational Chemistry*; Boyd, D. B., Lipkowitz, K., Eds.; Wiley: New York, 2003; pp 79−146.

(38) Hase, W. L.; Song, K.; Gordon, M. S. *Comput. Sci. Eng.* **2003**, *5*, 36.

(39) Wang, I. S. Y.; Karplus, M. *J. Am. Chem. Soc.* **1973**, *95*, 8160.

(40) Pople, J. A.; Santry, D. P.; Segal, G. A. *J. Chem. Phys.* **1965**, *43*, S129.

(41) Pople, J. A.; Segal, G. A. *J. Chem. Phys.* **1965**, *43*, S136.

(42) Hase, W. L.; Duchovic, R. J.; Hu, X.; Kormonicki, A.; Lim, K.; Lu, D.-H.; Peslherbe, G. H.; Swamy, K. N.; Linds, S. R. V.; Varandos, A. J. C.; Wang, H.; Wolf, R. J. *QCPE* **1996**, *16*, 671.

(43) Peslherbe, G. H.; Bolton, K.; Doubleday, C.; Hase, W. L. VENUS-MOPAC, A General Chemical Dynamics and Semiempirical Direct Dynamics Computer Program, to be released.

(44) Chapman, S.; Bunker, D. L. *J. Chem. Phys.* **1975**, *62*, 2890.

(45) Hase, W. L.; Ludlow, D. M.; Wolf, R. J.; Schlick, T. *J. Phys. Chem.* **1981**, *85*, 958.

(46) Press, W. H.; Teukolsky, S. A.; Vetterling, W. T.; Flannery, B. P. *Numerical Recipes in Fortran*; Cambridge University Press: Cambridge, U.K., 1992.

(47) The package can be provided by one of the authors, C.D., upon request.

(48) Camp, R. N.; King, H. F. *J. Chem. Phys.* **1981**, *75*, 268.

(49) Windus, T. L. Pacific Northwest National Laboratory, Richland, WA. Private communication, 2003.

(50) Barriers and heats of reaction were not calculated for the $CH_3O \rightarrow H_2 + HCO$ and $C_2H_5O \rightarrow CH_4 + HCO$ unimolecular decompositions. Using the experimental 0 K enthalpies from the NIST database (http://srdata.nist.gov/cccbdb), the 0 K heats of reaction for the former reaction is 5.0 kcal/mol. The PMP2/cc-pVTZ//UMP2/cc-pVTZ calculations give −1.5 and −12.4 kcal/mol for these 0 K heats of reaction. The reaction $C_2H_5O \rightarrow H_2 + CH_3-C\!\!=\!\!O$, also expected to be nearly thermoneutral, was not studied by the PMP2 calculations.

(51) Reid, J. P.; Marcy, T. P.; Kuehn, S.; Leone, S. R. *J. Chem. Phys.* **2000**, *113*, 4572.

(52) Alvarez-Idaboy, J. R.; Diaz-Acosta, I.; Vivier-Bunge, A. *J. Comput. Chem.* **1997**, *19*, 811.

(53) Levine, R. D.; Bernstein, R. B. *Chemical Reaction Dynamics and Chemical Reactivity*; Oxford University Press: New York, 1987.

(54) Lee, Y. T. In *Atomic and Molecular Beam Methods*; Scoles, G., Ed.; Oxford University Press: New York, 1988; Vol. 1.

(55) Troya, D.; Schatz, G. C.; Garton, D. J.; Brunsvold, A. L.; Minton, T. K. *J. Chem. Phys.* **2004**, *120*, 731.

(56) Troya et al.[14] stopped their trajectories when two products were separated by 6.3 Å. For H-atom elimination or abstraction, the integration time is less than 50 fs. For elimination of the heavier CH_3 radical, the integration time is expected to be less than 100 fs.